THE JOURNAL OF NAVIGATION (2019), **72**, 1481–1495.
doi:10.1017/S0373463319000328

Sensability and Excitability Metrics Applied to Navigation Systems Assessment

Martín España[1], Juan Carrizo[2] and Juan I. Giribet[2]

[1](*National Commission of Space Activities of Argentina (CONAE), Paseo Colon 751, 1063 Ciudad de Buenos Aires, Argentina*)
[2](*Department of Electronics, Faculty of Engineering, University of Buenos Aires, Paseo Colon 850, 1063 Ciudad de Buenos Aires, Argentina*)
(E-mail: mespana@conae.gov.ar)

To evaluate the aptness of a navigation system in a particular application, the designer needs to assess its performance over typical trajectories travelled by the vehicle itself. Moreover, he or she may be required to judge which components of the kinematics state may be better estimated (and which will not). The main contributions of this work are two novel and complementary performance measures that, in concert, allow for the assessment of a navigation system within the actual context of its application over specific trajectories. For a given on board instrumental configuration, the "excitability metric" permits the isolation of the contribution of the information conveyed by the vehicle's motion itself, while, the "sensability metric" measures the resultant overall quality of the kinematics state estimation. The same tools could help the designer planning appropriate vehicles manoeuvres in order to obtain a required precision for each estimated component. While emphasis is given on the mathematical justification of those metrics, their use is also illustrated with real flight data recorded from a sounding rocket.

KEYWORDS

1. Data fusion. 2. Excitability. 3. Sensability. 4. Suborbital rocket.

Submitted: 1 November 2018. Accepted: 10 April 2019. First published online: 4 June 2019.

1. INTRODUCTION. The objective of an embarked navigation system is to estimate, as precisely as possible, the components of a vehicle's kinematic state (attitude, position and velocity vectors) given all the available measurements on board. For several decades, real time estimation of a vehicle's kinematic state has been implemented through embedded navigation systems based on numerical filters fusing real time data coming from a variety of instruments included a core strap-down inertial measurement unit.

With respect to previously pure inertial navigation systems, multi-sensor integrated navigation systems allow for significant improvements in robustness, reliability, redundancy, costs and, of course, performance since the aggregation of independent measurements correlated with the state tends to reduce the covariance of its estimate. However, adding

instrumentation is never for free in terms of increasing uncertainties such as measurement noises, modelling errors and, of course, costs and computational requirements.

While evaluating the performance of an integrated navigation system, one may find that certain state components do not converge or that their covariances remain large. When errors in data acquisition, on the time-labelling or in the embedded software may be ruled out, it is natural to search the causes on the quality of the sensors, but also on the worth of the available information itself.

Sensor measurements are typically modelled by memory-less transduction functions parameterised by a set of parameters and additive disturbances, usually uncorrelated noise. Nominal values of sensors' parameters may be known in advance from the instrument data sheet provided by the manufacturer or else obtained through previous calibration procedures. Once the sensor's model structure is fixed, uncertainties are presumed concentrated on those parameters, which, multi-sensor fusion filters consider as part of an Augmented State Vector (ASV). However, sensor models are necessarily approximated; in particular, low performance sensors seldom obey a consistent mathematical model with stable parameters. Fusion filters deal with parameter instabilities by assuming they are perturbed by Brownian motions. The parametric components of the ASV are thus assumed permanently disturbed - the more so when low cost instruments are employed.

For a given instrument configuration, the measurements and the ASV become correlated through the kinematics differential equations of the vehicle's motion and the sensor models. To estimate the ASV, fusion filters (for example, Extended (EKF), Linear (LKF) and Unscented (UKF) Kalman Filters) make use of that correlation to produce a state estimate with its covariance matrix. The trace of the covariance matrix is often seen as a measure of the overall state estimate inaccuracy. However, for a high dimension ASV the correlation among its components hampers discerning which navigation variables may be better estimated (or better "sensed") with the available instrumentation. Ham and Brown (1983) pointed out the relevance that the eigen-structure of the covariance matrix has in addressing this issue. Further developing this idea, we here start from the singular value decomposition of the error covariance matrix to define a "practically sensable" subspace and its orthogonal complement, the "practically non-sensable" one. Based on this decomposition, a new instantaneous measure of the "sensability" of any linear combination of the ASV components is proposed as its orthogonal projection over the practically sensable subspace.

Deterministic "observability" (Willems and Mitter, 1971) designates the property and/or the conditions under which the state at a particular time may be determined from future measurable inputs and outputs. The non-linear nature of the kinematics equations makes observability in navigation systems strongly dependent on the vehicle's trajectory. Hence, besides measurement errors, sensors' parameter instabilities and uncertain initial conditions, the quality of the estimates depends on the actual vehicle's manoeuvres over different trajectory stretches. This motivated numerous analysis performed using ideal trajectories (lemniscates, circles, uniform acceleration, etc) so as to allow for a closed form analytical treatment of the problem (Bageshwar et al. (2009), Rhee et al. (2004) and Hoo et al. (2005) consider Inertial Navigation System (INS)/Global Positioning System (GPS) navigation systems). However, real vehicles' trajectories may rarely be analytically described or even predetermined. Shen et al. (2018) proposed a method (based on a Kalman scalar estimator algorithm pioneered by Salychev (1998)) for quantifying the observability of each state component over a given trajectory. Unfortunately, their approach requires the

https://doi.org/10.1017/S0373463319000328 Published online by Cambridge University Press

local Gramian observability matrix (denoted $\mathbf{O}_\tau$ in the text) to be well conditioned over the considered trajectory.

A new "excitability measure" is proposed here to quantify the information, relative to the initial state, conveyed by the innovations during any given trajectory stretch. This is done based on a synthetic trajectory (Giribet et al., 2007) determined from actual flight data. Linearized models of state deviations and innovations are determined by referring to this synthetic trajectory. Once more, a principal component analysis, this time of the deterministic innovation signals, over any time interval, allows us to decompose the initial ASV state space (of any given trajectory stretch) into a Practically Observable Subspace (POS) and its orthogonal complement: the "practically un-observable subspace". The new measure of the excitability for any vector (physical state components included) of the initial state space is defined as the norm of its orthogonal projection onto the POS. Notice that, contrary to other approaches, the excitability measure empirically qualifies any given vehicle's trajectory stretch; that is, it is not the result of an *ad hoc* analysis of a pre-assumed manoeuvre (as for instance in Tang et al., 2009).

The paper is organised as follows: Section 2 presents the mathematical formulation and main notation used in the paper; practical sensability and practical observability subspaces for the ASV are introduced, respectively, in Sections 3 and 4 whereby the sensability and excitability metrics are established.

In Section 5, these concepts are used to assess the performance navigation results with actual flight data from CONAE's (National Commission of Space Activities: Argentina's Space Agency) first experimental navigation payload on a suborbital rocket. Finally, Section 6 concludes the paper.

2. MATHEMATICAL FORMULATION. A causal non-linear filter reconstructs the present state given past measurements. An integrated navigation algorithm is a particular case of nonlinear filtering based on kinematics equations which, when using the Earth-Centred-Earth-Fixed (ECEF) frame as the reference frame, adopts the following form (see for example, España (2017)):

$$\begin{aligned}
\dot{\mathbf{P}}^e &= \mathbf{V}^e \\
\dot{\mathbf{V}}^e &= \mathbf{C}_b^e \mathbf{f}^b + \gamma^e(\mathbf{P}^e) - 2(\boldsymbol{\Omega}^e \times \mathbf{V}^e);\ \mathbf{C}_b^e = \exp(\mathbf{S}(\boldsymbol{\theta}_{be})) \\
\dot{\boldsymbol{\theta}}_{be} &= \boldsymbol{\omega}_{eb}^e + \frac{1}{2}\boldsymbol{\theta}_{be} \times \boldsymbol{\omega}_{eb}^e + \left(1 - \frac{\theta_{be}\sin\theta_{be}}{2(1-\cos\theta_{be})}\right)\breve{\boldsymbol{\theta}}_{be} \times \left(\breve{\boldsymbol{\theta}}_{be} \times \boldsymbol{\omega}_{eb}^e\right) \\
\boldsymbol{\omega}_{eb}^e &= \boldsymbol{\omega}_{ib}^e - \boldsymbol{\omega}_{ie}^e = \mathbf{C}_b^e \boldsymbol{\omega}_{ib}^b - \boldsymbol{\Omega}^e
\end{aligned} \tag{1}$$

where: $\mathbf{P}^e, \mathbf{V}^e$ are the vehicle's position and velocity in the ECEF frame; $\boldsymbol{\theta}_{be}$ and $\mathbf{C}_b^e$ are, respectively, the vector angle and the rotation matrix relating the ECEF frame and the body frame; the specific force $\mathbf{f}^b$ and the angular rate $\boldsymbol{\omega}_{ib}^b$, both projected onto the body's frame, are gathered in the inertial magnitude vector $\boldsymbol{\mu} \triangleq \left[\mathbf{f}^{b\prime}\boldsymbol{\omega}_{ib}^{b\prime}\right]'$, ($(')$ stands for transpose), $\gamma^e(\mathbf{P}^e)$ is the local gravity as a function of the vehicle's position, both in Earth Cartesian coordinates and $\boldsymbol{\Omega}^e$ is the Earth angular rate. By using the Inertial Measurement Unit (IMU) inverse model and assuming additive disturbances ξ_μ (España, 2017), $\boldsymbol{\mu}$ may

https://doi.org/10.1017/S0373463319000328 Published online by Cambridge University Press

be expressed as a function of its measured value $\widehat{\boldsymbol{\mu}}$ as:

$$\boldsymbol{\mu} = \mathcal{M}(\widehat{\boldsymbol{\mu}}; \mathbf{p}_i) = \xi_\mu; \tag{2}$$

The inertial as well as the exteroceptive instruments' models are characterised by a vector of unknown parameters $\mathbf{p} \triangleq [\mathbf{p}_i' \ \mathbf{p}_e']'$ with assumed known expected values. The kinematics state vector $\mathbf{x} \triangleq [\mathbf{P}^{e\prime} \ \mathbf{V}^{e\prime} \ \theta_{be}']'$ and the instrument parameters vector $\mathbf{p}$ are compounded in the ASV defined as $\boldsymbol{\chi} \triangleq [\mathbf{x}' \ \mathbf{p}']' \in \mathbb{R}^n$. When $\mathbf{p}$ is modelled as a Brownian motion (Farrell, 2008), $\boldsymbol{\chi}$ may be modelled by the following stochastic equation, affine in the perturbations $\boldsymbol{\xi}(t)$:

$$\begin{aligned} \dot{\boldsymbol{\chi}} &= \begin{bmatrix} \dot{\mathbf{x}} \\ \dot{\mathbf{p}} \end{bmatrix} = \overbrace{\begin{bmatrix} \mathbf{f}_{kin}(\boldsymbol{\chi}; \widehat{\boldsymbol{\mu}}(t)) \\ 0 \end{bmatrix}}^{\mathcal{F}(\boldsymbol{\chi};t)} + \overbrace{\begin{bmatrix} \mathbf{B}_{kin}(\mathbf{x}) & 0 \\ 0 & I \end{bmatrix}}^{\mathbf{B}(\mathbf{x})} \overbrace{\begin{bmatrix} \boldsymbol{\xi}_\mu \\ \boldsymbol{\xi}_p \end{bmatrix}}^{\xi(t)}; \\ \widehat{\mathbf{y}}_k &= \mathbf{h}_k(\boldsymbol{\chi}(t_k)) + \eta_k \end{aligned} \tag{3}$$

where $\mathbf{h}_k(\cdot)$ models the active exteroceptive instruments producing the measurement vector $\widehat{y}_k$ at time t_k; η_k is a discrete time white disturbance with known diagonal covariance matrix $\mathbf{R}_k$; the noise ξ_p models the sensor's parameters instabilities; ξ_μ and ξ_p are continuous white noises with assumed known Power Spectral Densities (PSD), respectively: $\mathbf{S}_\mu$, $\mathbf{S}_p$.

For t_0 as the starting time of an arbitrary trajectory stretch, the initial state $\boldsymbol{\chi}(t_0)$ in Equation (3) is a random vector with the first two moments $\hat{\boldsymbol{\chi}}_0 = E\{\boldsymbol{\chi}(t_0)\}$, $\mathbf{P}_0 = \mathrm{cov}(\boldsymbol{\chi}(t_0))$ provided by the navigation algorithm being assessed. When t_0 is the initial navigation time, $\hat{\boldsymbol{\chi}}_0$, $\mathbf{P}_0$ reflect the vehicle's alignment procedure and $\mathbf{P}_0$ is normally assumed diagonal.

Given a reference solution of the nonlinear model Equation (3), denoted as $\boldsymbol{\chi}_r(t)$, we introduce the state deviations $\delta\boldsymbol{\chi}(t) \triangleq \boldsymbol{\chi}(t) - \boldsymbol{\chi}_r(t)$ and the innovations $\delta\mathbf{y}_k \triangleq \bar{\mathbf{y}}_k - \mathbf{h}_k(\boldsymbol{\chi}_r(t_k))$, which, for smooth enough $\mathbf{f}_{kim}$, $\mathbf{h}_k$ and small enough perturbations and initial state errors, may be modelled by the following time varying linear equations:

$$\begin{cases} \delta\dot{\boldsymbol{\chi}} = \mathbf{A}(\boldsymbol{\chi}_r, \widehat{\mu})\delta\boldsymbol{\chi} + \mathbf{B}(\mathbf{x}_r)\boldsymbol{\xi}; \quad \delta\boldsymbol{\chi}(t_0) \sim \left(\delta\hat{\boldsymbol{\chi}}_0, \mathbf{P}_0\right) \\ \delta\mathbf{y}_k = \mathbf{H}_k\left(\boldsymbol{\chi}_r(t_k)\right)\delta\boldsymbol{\chi}(t_k) + \eta_k \end{cases} \tag{4}$$

where $\mathbf{A}(\cdot)$ and $\mathbf{H}_k(\cdot)$ are the partial derivatives matrices with respect to $\boldsymbol{\chi}$, respectively, of $\mathcal{F}(\boldsymbol{\chi}; t)$ and $\mathbf{h}_k(\boldsymbol{\chi})$ in model Equation (3) evaluated along the reference trajectory.

When restricted to the kinematic state, from Equations (1), the deviation equations are given by (see, for example, España (2017), Equation 6.22).

$$\begin{aligned} \delta\dot{\mathbf{x}} &= \begin{bmatrix} 0 & \mathbf{I}_3 & 0 \\ \gamma_P^e\big|_{P^e} & -2\mathbf{S}(\boldsymbol{\Omega}_e^e) & -\hat{\mathbf{C}}_\mathbf{b}^\mathbf{e}\mathbf{S}(\hat{\mathbf{f}}^e) \\ 0 & 0 & -\mathbf{S}(\bar{\boldsymbol{\omega}}_{ib}^e) \end{bmatrix} \begin{bmatrix} \delta\mathbf{P}^e \\ \hline \delta\mathbf{V}^e \\ \hline \delta\boldsymbol{\theta}_{be} \end{bmatrix} + \begin{bmatrix} 0 & 0 \\ 0 & \hat{\mathbf{C}}_\mathbf{b}^\mathbf{e} \\ \mathbf{I} & 0 \end{bmatrix} \delta\boldsymbol{\mu} \\ &= \mathbf{A}_{kin}(t)\delta\mathbf{x} + \mathbf{B}_{kin}(t)\delta\boldsymbol{\mu}; \quad \delta\mathbf{x}(t_0) \sim (\delta\hat{\mathbf{x}}_0, \mathbf{P}_{x0}) \\ \delta\boldsymbol{\mu} &= \mathbf{B}_{p_i}(\widehat{\boldsymbol{\mu}})\delta\mathbf{p}_i + \boldsymbol{\xi}_\mu \end{aligned} \tag{5}$$

https://doi.org/10.1017/S0373463319000328 Published online by Cambridge University Press

where: $\mathbf{S}:\mathbb{R}^3\rightarrow\mathbb{R}^{3\times3}$ is the vector product matrix operator; γ_P^e the Jacobian of the normal gravity with respect to $\mathbf{P}^e$; $\delta\mathbf{P}^e, \delta\mathbf{V}^e, \delta\boldsymbol{\theta}_{be}$, are the components of the kinematics state deviations vector and $\delta\boldsymbol{\mu}$ the IMU's deviation measurement vector, with $\mathbf{B}_{p_i}(\hat{\boldsymbol{\mu}})$ the Jacobian of $\mathcal{M}$ (in Equation (2)) with respect to $\mathbf{p}_i$.

The solution to the linear time varying differential Equation (4) in the interval $[t_k\ t_{k+1}]$ between two consecutive exteroceptive measurement acquisition times, is given by (Farrell, 2008):

$$\begin{aligned}&\delta\boldsymbol{\chi}(t_{k+1})=\boldsymbol{\Phi}(t_{k+1},t_k)\delta\boldsymbol{\chi}(t_k)+\boldsymbol{\varepsilon}_k;\boldsymbol{\varepsilon}_k\triangleq\int_{t_k}^{t_{k+1}}\boldsymbol{\Phi}(t_{k+1},\tau)\mathbf{B}(\tau)\boldsymbol{\xi}(\tau)d\,\tau\\&\dot{\boldsymbol{\Phi}}(t,t_0)=\mathbf{A}(t)\boldsymbol{\Phi}(t,t_0);\boldsymbol{\Phi}(t_0,t_0)=I\end{aligned}\tag{6}$$

where $\boldsymbol{\Phi}(\cdot,\cdot)\in\mathbb{R}^{n\times n}$ is the state transition matrix of the time varying linear system Equation (4) and $\boldsymbol{\varepsilon}_k$ is a centred uncorrelated random sequence such that:

$$E\left[\boldsymbol{\varepsilon}_j\boldsymbol{\varepsilon}_k^T\right]=\mathbf{Q}_k\delta_{jk};E\left[\boldsymbol{\varepsilon}_j\boldsymbol{\eta}_k^T\right]=0;\quad\forall j,k\tag{7}$$

The positive definite covariance matrix $\mathbf{Q}_k$ is obtained by introducing the power spectral density (Starks and Woods, 1994) $\mathbf{S}=diag\left(\mathbf{S}_\mu,S_p\right)$ in the integral expression of $\boldsymbol{\varepsilon}_k$ given in Equation (6) (see España (2017) for details) and δ_{jk} stands for the Kronecker delta. Denoting the non-singular matrix $\mathbf{F}_k=\boldsymbol{\Phi}(t_{k+1},t_k)$ and $\delta\boldsymbol{\chi}_k=\delta\boldsymbol{\chi}(t_k)$, with Equation (6), the discrete time models for the ASV and the innovation are rewritten as:

$$\begin{cases}\delta\boldsymbol{\chi}_{k+1}=\mathbf{F}_k\delta\boldsymbol{\chi}_k+\varepsilon_k;\delta\boldsymbol{\chi}_0\sim\left(\delta\hat{\boldsymbol{\chi}}_0,\mathbf{P}_0\right)\\\delta\mathbf{y}_k=\mathbf{H}_k\delta\boldsymbol{\chi}_k+\eta_k\end{cases}\tag{8}$$

The EKF refers the state deviations to the *a priori* estimate $\hat{\boldsymbol{\chi}}_{k+1}^-$ calculated at the end of the k-th interval by numerical integration of model Equation (3) after substitution of all random variables by their expected values, that is: $\boldsymbol{\xi}\rightarrow0$; $\boldsymbol{\chi}(t_k)\rightarrow\hat{\boldsymbol{\chi}}_k$ -the last one being the previous *a posteriori* estimate obtained at the beginning of the k-th interval. This procedure, first introduced by Jazwinski (1970), is known as the Certainty Equivalence Principle. Once the next measurement becomes available, the *a posteriori* estimate $\hat{\boldsymbol{\chi}}_{k+1}$ is obtained, updating the prediction $\hat{\boldsymbol{\chi}}_{k+1}^-$ by adding the innovation: $\bar{\mathbf{y}}_{k+1}-\mathbf{h}_k(\hat{\boldsymbol{\chi}}_{k+1}^-)$ multiplied by the Kalman gain calculated as (Anderson and Moore, 1979):

$$\mathbf{K}_k=\mathbf{P}_k^-\mathbf{H}_k^T\left(\mathbf{H}_k\mathbf{P}_k^-\mathbf{H}_k^T+\mathbf{R}_k\right)^{-1}=\mathbf{P}_k\mathbf{H}_k^TR_k^{-1}\tag{9}$$

where $\mathbf{P}_k^-=E(\boldsymbol{\chi}_k-\hat{\boldsymbol{\chi}}_k^-)(\boldsymbol{\chi}_k-\hat{\boldsymbol{\chi}}_k^-)^T$ and $\mathbf{P}_k=E\left(\boldsymbol{\chi}_k-\hat{\boldsymbol{\chi}}_k\right)\left(\boldsymbol{\chi}_k-\hat{\boldsymbol{\chi}}_k\right)^T$ are, respectively, the *a priori* and the *a posteriori* covariances of the state error modelled by Equation (8). We introduce the *a priori* and *a posteriori* information matrices: $\mathcal{I}_k^-\triangleq(\mathbf{P}_k^-)^{-1}$, $\mathcal{I}_k\triangleq\mathbf{P}_k^{-1}$. As shown in Anderson and Moore (1979) or Jazwinski (1970), both matrices may be determined with the next recursive equations starting from $\mathcal{I}_0^{-1}=\mathbf{P}_0>0$.

$$\begin{aligned}&a)\ \mathbf{P}_{k+1}^-=\mathbf{F}_k\mathbf{P}_k\mathbf{F}_k^T+\mathbf{Q}_k;&&\leftarrow\text{covariance propagation}\\&b)\ \mathcal{I}_{k+1}=\mathcal{I}_{k+1}^-+\mathbf{H}_{k+1}^T\mathbf{R}_{k+1}^{-1}\mathbf{H}_{k+1};&&\leftarrow\text{information update}\end{aligned}\tag{10}$$

From Equations (10), the current state accuracy at any time t_k is the consequence of two opposed effects. The first one, called "disturbability" by Bryson (1978), concerns

https://doi.org/10.1017/S0373463319000328 Published online by Cambridge University Press

the growth of the state uncertainty due to the disturbance covariance noise matrix $\mathbf{Q}_k$ (Equation (10a)). The second one, called "estimability" by Baram and Kailath (1988) regards the growth of the information matrix produced by the new measurement acquired at time t_{k+1} (Equation (10b). Both effects depend on the Jacobians $\mathbf{A}(\cdot)$, $\mathbf{H}(\cdot)$ and $\mathbf{B}(\cdot)$ evaluated over the reference trajectory. As such, the accuracy of the ASV estimate depends on: (a) the performance of the onboard instruments (through the inertial sensor's PSD $\mathbf{S}$ and external measurement noise $\mathbf{R}_k$), (b) the initial state errors covariance $\mathbf{P}_0$ and (c) the vehicle's trajectory itself (Giribet et al., 2018).

Since the components of $\delta\boldsymbol{\chi}_k$, $\delta\mathbf{y}_k$ and those of the corresponding driving noises are expressed in different physical units, their magnitudes are not directly comparable. Thus, for $\mathbf{D}_0 \triangleq diag(\mathbf{P}_0)$ and $\mathbf{R}_0$ assumed diagonal, we proceed to normalise ("dedimensionalise") model Equation (8) through the following change of variables (Krener and Kayo, 2009):

$$\delta\boldsymbol{\chi}_k \rightarrow \mathbf{D}_0^{-1/2}\delta\boldsymbol{\chi}_k; \delta\mathbf{y}_k \rightarrow \mathbf{R}_0^{-1/2}\delta\mathbf{y}_k \tag{11}$$

With variable change Equation (11), matrices in Equation (8) are transformed as: $\mathbf{F}_k \rightarrow \mathbf{D}_0^{1/2}\mathbf{F}_k\mathbf{D}_0^{1/2}$; $\mathbf{H}_k \rightarrow \mathbf{R}_0^{-1/2}\mathbf{H}_k\mathbf{D}_0^{1/2}$. Thus, the new normalised state deviations' covariance transforms as: $\mathbf{P}_k \rightarrow \mathbf{D}_0^{-1/2}\mathbf{P}_k\mathbf{D}_0^{-1/2}$; $\forall k$, while the output additive error noise covariance as: $\mathbf{R}_k \rightarrow \mathbf{R}_0^{-1/2}\mathbf{R}_k\mathbf{R}_0^{-1/2}$; $\forall k$. Moreover, with $\mathbf{Q}_k \rightarrow \mathbf{D}_0^{-1/2}\mathbf{Q}_k\mathbf{D}_0^{-1/2}$, a simple substitution shows that the new normalised matrix $\mathbf{P}_k$ still satisfies the recursive Equations (10). We call $\mathcal{E} \triangleq \left\{\mathbf{e}^i : i = 1, 2, \ldots, n\right\}$ the canonical base in which the physical but dimensionless state is represented after transformation Equation (11).

$\mathcal{I}_k$, a real symmetric positive definite matrix for any k, may be decomposed into a diagonal form, such as $\mathcal{I}_k = \mathbf{V}_k\Lambda_k\mathbf{V}_k^T$ where, $\Lambda_k = diag(\lambda_k^1, \lambda_k^2, \ldots, \lambda_k^n)$ is built with the ordered set of $\mathcal{I}_k$'s eigen-values: $\left\{\lambda_k^1 \geq \lambda_k^2 \geq \cdots \geq \lambda_k^n > 0\right\}$ and $\mathbf{V}_k = \left[\mathbf{v}_k^1 \mid \mathbf{v}_k^2 \mid \ldots \mid \mathbf{v}_k^n\right] \in \mathbb{R}^{nxn}$ is the matrix with, as columns, the set of $\mathcal{I}_k$'s unit orthogonal right eigen-vectors. In what follows, it is assumed that there exists $0 < \underline{p} < \bar{p} < \infty$ such that for all t_k $\underline{p} < \lambda_k' < \bar{p}$, $i = 1, \ldots, n$. This ensures that there is no numerical divergence on recursion Equations (10) and also that there are no purely deterministic directions in the state space (see next section).

3. RELATIVE SENSABILITY: SUBSPACES AND METRICS.

Assuming the $\mathbf{v}_k^i$ expressed in the canonical base $\mathcal{E}$ in which the normalised augmented physical state model Equation (8) is represented, we introduce the transformation $\delta\boldsymbol{\chi}_k \rightarrow \delta\mathbf{z}_k$ in $\mathbb{R}^n$ defined as:

$$\delta\mathbf{z}_k = \mathbf{V}_k^T\delta\boldsymbol{\chi}_k; \tag{12}$$

The component δz_k^i of $\delta\mathbf{z}_k$ is the projection of the state deviation vector $\delta\boldsymbol{\chi}_k$ ("physical" normalised coordinates) over the i-th $\mathcal{I}_k$'s eigen-vector. At each instant t_k the covariance matrix of the transformed vector is:

$$\begin{aligned} \mathrm{Cov}\,(\delta\mathbf{z}_k) &= \mathbf{V}_k^T\, E\left\{\delta\boldsymbol{\chi}_k\delta\boldsymbol{\chi}_k{}^T\right\}\mathbf{V}_k \\ &= \mathbf{V}_k^T\mathbf{P}_k\mathbf{V}_k = \left(\mathbf{V}_k^T\mathcal{I}_k\mathbf{V}_k\right)^{-1} = \Lambda_k^{-1} \end{aligned} \tag{13}$$

https://doi.org/10.1017/S0373463319000328 Published online by Cambridge University Press

From Equations (12) and (13) the transformed state deviation components are orthogonal random variables satisfying:

$$\begin{aligned} &i)\ E\left\{\delta z_k^i \delta z_k^i\right\} = 0 \quad \forall i \neq j \\ &ii)\ E\left\{(\delta z_k^i)^2\right\} = 1/\lambda_k^i \\ &iii)\ E\left\{\|\delta \mathbf{z}_k\|^2\right\} = E\left\{\left\|\delta \boldsymbol{\chi}_k\right\|^2\right\} = \sum\nolimits_i 1/\lambda_k^i = tr(\mathbf{P}_k) \end{aligned} \tag{14}$$

Each standard deviation $\sqrt{1/\lambda_k^i}$ being the state uncertainty along the eigen-direction $\mathbf{v}_k^i$, $\sqrt{tr(\mathbf{P}_k)}$ is a measure of the instantaneous "total state uncertainty". Symmetrically, $\sqrt{tr(\mathcal{I}_k)}$ is seen as a measure of the "total state accuracy". Given the ordering of the λ_k''s, the state space direction best estimated (least variance) is the first principal component (pc) $\mathbf{v}_k^1$ of the information matrix $\mathcal{I}_k$ with $\mathrm{Cov}\left(\delta z_k^1\right) = 1/\lambda_k^1$; the next best estimated is $\mathbf{v}_k^2$ and so on until $\mathbf{v}_k^n$.

We now consider the sets of sequentially embedded subspaces $\mathcal{V}_k^i \triangleq span\left\{\mathbf{v}_k^1, \mathbf{v}_k^2, \ldots, \mathbf{v}_k^i\right\}$ $\left(\mathcal{V}_k^{i+1} \supset \mathcal{V}_k^i\right)$ and introduce the following ratios monotonously increasing with i towards $r^n = 1$.

$$r_k^i = \sqrt{\sum_{j=1}^{i} \lambda_k^j \Big/ \sum_{j=1}^{n} \lambda_k^j} : i = 1, 2, \ldots, n \tag{15}$$

If, for a given $i \leq n$, $r^i \approx 1$, it means that the subspace $\mathcal{V}_k^i$ contains the *pc*s that concentrates the major part of the total accuracy of the estimator. Given this, we introduce:

Definition 1: For a threshold $0 < \nu < 1$ empirically chosen close to 1, we denote *nr* the first index i in Equation (15) such that $r_k^{nr} \geq \nu$ and call $S_k^s \equiv \mathcal{V}_k^{nr}$ the *practically sensable (ps) subspace* and $S_k^{NS} \equiv (S_k^S)^{\perp}$ the *practically non-sensable (pns) subspace* to its orthogonal complement.

By definition, the random components of δz_i over S_k^S are the *ps* ones. Since $\mathbb{R}^n = S_k^S \oplus S_k^{NS}$, on any t_k, each element $\mathbf{e}_i$ of the canonical (physical) base may be decomposed into its orthogonal projections $\pi_s(\mathbf{e}_i)_k$ and $\pi_{ns}(\mathbf{e}_i)_k$, respectively, over S_k^S and S_k^{NS} as:

$$\mathbf{e}_i = \sum_{\mathbf{v}_j \in S_k^s} \left\langle \mathbf{e}_i, \mathbf{v}_j \right\rangle \mathbf{v}_j + \sum_{\mathbf{v}_l \in S_k^{ns}} \langle \mathbf{e}_i, \mathbf{v}_l \rangle \, \mathbf{v}_l \triangleq \pi_s\left(\mathbf{e}_i\right)_k + \pi_{ns}\left(\mathbf{e}_i\right)_k \tag{16}$$

Definition 2: $s_k^i \triangleq \|\pi_s(\mathbf{e}_i)_k\|$ is the *practical sensability* instantaneous measure of the ASV's *i*-th component.

Some practical considerations on the choice of the threshold ν are in order. It is assumed that at least one component of the ASV is *ps* (otherwise the instrumentation should be reviewed) so, whenever the λ_k^i's are similar ($\lambda_{ki}^i \approx \bar{\lambda}_k, \forall i$) one expects that all the ASV components be *ps* (that is: $S_k^s = \mathcal{V}_k^n$). Now, since in this case $r_k^i \approx \sqrt{i/n}$, it needs to be $\nu \in (1 - 1/n, 1)$, or else, one may have $r_k^{n-1} > \nu$ meaning that the last component is *pns*, which is contrary to the assumption. Thus, for a small enough ε empirically chosen, we propose the dimensionally dependent choice of $\nu = \sqrt{1 - 1/n + \varepsilon} < 1$.

https://doi.org/10.1017/S0373463319000328 Published online by Cambridge University Press

Notice that decomposition Equation (16) is generically time variant, which means that some eigen-directions may go in and out of the subspace S_k^S. As such, its associated measure may change with time depending on previous data. This motivates quantifying the available information embedded in a given vehicle's trajectory segment, which is the subject of the next section. Our point of view differs here once more with respect to that of Tang et al. (2009) in the sense that we search to study, segment by segment, the actual vehicle's trajectory.

4. OBSERVABILITY AND THE EXCITABILITY METRIC. Contrary to the sensability metric which is evaluated at each time t_k, we now seek to assess the actual information conveyed by the innovations along a given time interval. The measure we look for is not intended to depend on the instrumentation performance but to meet the practical need of quantifying the impact of vehicles' manoeuvres on the estimability of the ASV, for a given instrument configuration.

The analysis is performed by first synthesising a deterministic trajectory with corresponding measurements signals (inertial and exteroceptive). The method, proposed by Giribet et al. (2007), produces the smooth B-spline exactly satisfying the kinematics Equations (1) that best fits the flight data in the a mean square sense. The measurements are calculated with Equation (2) assuming perfect instruments, that is: $\boldsymbol{\xi}_\mu = 0$, $\boldsymbol{\xi}_p = 0\ \forall t$, $\eta_k = 0 \forall t_k$ and also $\boldsymbol{\varepsilon}_k = 0$ in Equation (6). The synthetic trajectories and measurements are then used as references to construct the linearized state deviations and innovation models in Equations (4), (5) and (8).

4.1. *Observability analysis.* Given the above assumptions, the innovations on the set of time instants $\tau = \{t_0, t_1, \ldots, t_N\}$ modelled by Equation (8) may be expressed as a linear function of the initial state deviation as:

$$\mathbf{Y}_\tau(\delta\mathbf{x}_0) = \begin{bmatrix} \mathbf{y}(t_0) \\ \mathbf{y}(t_1) \\ \cdots \\ y(t_{N-1}) \end{bmatrix} = \begin{bmatrix} \mathbf{H}_0 \\ \mathbf{H}_1\mathbf{F}_0 \\ \cdots \\ \mathbf{H}_{N-1}\mathbf{F}_{N-2}\cdots\mathbf{F}_1\mathbf{F}_0 \end{bmatrix} \delta\boldsymbol{\chi}_0 \triangleq \mathbf{O}_\tau \delta\boldsymbol{\chi}_0 \tag{17}$$

The matrix $\mathbf{O}_\tau \in \mathbb{R}^{(pN)\times n}$ was called the extended observability matrix by Moore (1981). If a null linear combination were to exist among the n columns of $\mathbf{O}_\tau$ a whole non-zero subspace of the initial deviations state-space would be mapped into the null innovation signal. Accordingly, the largest subspace of $\mathbb{R}^n$ contained in the kernel of $\mathbf{O}_\tau$ is the unobservable subspace of the system Equation (8) within the interval τ. When the unobservable subspace is reduced to the origin, the system Equation (8) is said to be completely observable. Observability is thus a binary condition stating whether or not the innovations carry total information about the initial state deviations. Unfortunately, this does not give us a hint of which state components may be better determined and, more importantly, in what amount.

4.2. *Principal components of the innovation signal.* We now introduce the *Observability Gramian* for the interval τ: $\mathbf{M}_\tau \triangleq \mathbf{O}_\tau^T\mathbf{O}_\tau \in \mathbb{R}^{n\times n}$. Being a symmetric non-negative definite matrix, there exists a set $B_\tau = \left\{\mathbf{u}_\tau^i \in \mathbb{R}^n : i = 1, 2, \ldots, n\right\}$ of unitary, mutually orthogonal eigenvectors associated with the ordered set $\left\{\sigma_\tau^1 \geq \sigma_\tau^2 \geq \ldots \geq \sigma_\tau^n\right\}$ of non-negative eigen-values (all positives only if system Equation (8) is completely observable, that is: $\mathbf{M}_\tau$ is non-singular). With the elements of B_τ expressed in coordinates of the

https://doi.org/10.1017/S0373463319000328 Published online by Cambridge University Press

canonical base, the orthogonal matrix $\mathbf{U}_\tau = \left[\mathbf{u}_\tau^1 \mid \mathbf{u}_\tau^2 \mid \ldots \mid \mathbf{u}_\tau^n\right] \in \mathbb{R}^{ncn}$ leads to the similarity transformation $\mathbf{M}_\tau = \mathbf{U}_\tau^T \mathbf{\Sigma}_\tau \mathbf{U}_\tau$ for $\mathbf{\Sigma}_\tau \triangleq diag\left\{\sigma_\tau^1, \sigma_\tau^2, \ldots, \sigma_t^n\right\}$. Using the fact that $\sum_i \mathbf{u}_\tau^i \mathbf{u}_\tau^{iT} = I_n$, we write:

$$\mathbf{O}_\tau = \mathbf{O}_\tau \left(\sum_i \mathbf{u}_\tau^i \mathbf{u}_\tau^{iT} \right) = \sum_i \mathbf{o}_\tau^i \mathbf{u}_\tau^{iT} \tag{18}$$

The set of responses to the initial state deviations $\mathbf{u}_\tau^i$: $\mathbf{o}_\tau^i \triangleq \mathbf{O}_\tau \mathbf{u}_\tau^i = \mathbf{Y}_\tau(\mathbf{u}_\tau^i)$, $i = 1, \ldots, n$, are called the *innovation signal principal components (ispc)* in τ. As can be shown, they are mutually orthogonal (that is: $\mathbf{o}_\tau^{iT} \mathbf{o}_\tau^j = \sigma_\tau^j \delta_{ij}$) and such that $\|\mathbf{o}_\tau^i\|^2 = \sigma_\tau^i$. Moreover, for any initial state $\delta\boldsymbol{\chi}_0 = \sum_i \alpha_i \mathbf{u}_\tau^i$ represented in B_τ coordinates, the innovation signal is expressed by the same linear combination of the *ispcs*, that is: $\mathbf{Y}_\tau(\delta\boldsymbol{\chi}_0) = \sum_i \alpha_i \mathbf{o}_\tau^i$. On the other hand, for a given innovation signal over an interval τ, the components on B_τ of the initial state may be recovered through: $\alpha_i = (\mathbf{Y}_\tau^T \mathbf{o}_\tau^i)/\sigma_\tau^i$ provided that $\sigma_\tau^i \neq 0$. This just restates the fact that an unobservable subspace exists in τ whenever $\sigma_\tau^n = 0$.

By using the orthogonality of the $\mathbf{0}_\tau^i$ s, one shows that the total energy of the output signal over τ, given by: $E_\tau(\delta\boldsymbol{\chi}_0) \triangleq \|\mathbf{Y}_\tau(\delta\boldsymbol{\chi}_0)\|^2 = \sum_i \alpha_i^2 \|\mathbf{o}_\tau^i\|^2$, which may also be decomposed into a linear combination of the individual *ispc's* energies: $E_\tau(\mathbf{u}_\tau') = \|\mathbf{o}_\tau'\|^2 = \sigma_\tau^i$, with, as coefficients, the squares of the initial state components in B_τ. Clearly, the combined energy of all the *ispcs* within τ is $tr(\mathbf{M}_\tau)$.

4.3. *An excitability metric.* We now consider the mapping sending any point of the (unit) n-hypersphere S^n into $\mathbb{R}^n$: $\mathbf{e}_\tau(\mathbf{v}) = E_\tau(\mathbf{v})\mathbf{v}$ with $\|\mathbf{v}\| = 1$. Its image $\mathbf{e}_\tau(S^n)$ describes an n-hyper-ellipsoid E^n with axes $\sigma_i^\tau \mathbf{u}_\tau^i$; $i = 1, \ldots, n$. The radius vector to each point on E^n measures the sensitivity of the innovation's energy to an initial state deviation in that particular direction. The maximum sensitivity is σ_τ^1 attained in the direction of $\mathbf{u}_\tau^1$.

In practice, for a given vehicle's trajectory and time interval τ, one may expect that the innovation's energy will be almost insensitive to some directions in S^n. This motivates establishing a criterion to decide which directions contribute to the innovations and which do not.

Considering that $tr(\mathbf{M}_\tau)/n$ is the average energy induced by the $\mathbf{u}_\tau^i$s, we introduce the relative excitability index of the direction $\mathbf{v}$ on S^n:

$$S_\tau(\mathbf{v}) \triangleq \frac{n}{tr(\mathbf{M}_\tau)} \sum\nolimits_i \alpha_i^2 \sigma_\tau^i; \quad \|\mathbf{v}\|^2 = \sum\nolimits_i \alpha_i^2 = 1 \tag{19}$$

Now, if for a sufficiently small number η, empirically chosen, there exists an index $ne \in \{1, \ldots, n\}$ such that:

$$S_\tau(\mathbf{u}_\tau^{ne}) \leq \eta; 0 < n \ll 1; \textit{ for some ne} \tag{20}$$

then, that means that the contribution of the components $\mathbf{u}_\tau^{ne}, \ldots, \mathbf{u}_\tau^n$ to the total energy $tr(\mathbf{M}_\tau)$ may be neglected. This establishes a partition in the orthogonal set $\{\mathbf{u}_\tau^i\}$, which in turn determines the orthogonal complementary subspaces:

$$\begin{aligned} S_\tau^O &\equiv span\{\mathbf{u}_\tau^i; i < ne\} \\ S_\tau^{NO} &= S_\tau^{O\perp} \equiv span\{\mathbf{u}_\tau^i; i \geq ne\} \end{aligned} \tag{21}$$

Definition 3: S_τ^O is called the *practically observable* subspace and the *practically non-observable* one.

https://doi.org/10.1017/S0373463319000328 Published online by Cambridge University Press

Since $\mathbb{R}^n = S_\tau^O \oplus S_\tau^{NO}$, as in Equation (16), each element $\mathbf{e}^i$ of the canonical base $\mathcal{E}$ is decomposed into its orthogonal projections $\pi_\tau^O(\mathbf{e}^i)$ and $\pi_\tau^{NO}(\mathbf{e}^i)$ respectively over S_τ^O and S_τ^{NO}:

$$\mathbf{e}^i = \sum_{\mathbf{u}_\tau^j \in S_\tau^O} \left\langle \mathbf{e}^i, \mathbf{u}_\tau^j \right\rangle \mathbf{u}_\tau^j + \sum_{\mathbf{u}_\tau^j \in S_\tau^{NO}} \left\langle \mathbf{e}^i, \mathbf{u}_\tau^j \right\rangle \mathbf{u}_\tau^j \triangleq \pi_\tau^O(\mathbf{e}^i) + \pi_\tau^{NO}(\mathbf{e}^i) \tag{22}$$

Definition 4: $e_\tau^i \triangleq \|\pi_\tau^O(\mathbf{e}^i)\|$ is the practical excitabilty metric of the ASV's *i*-th component over the interval τ.

Notice that (contrary to Shen et al. (2018)) no *a priori* claim on the conditioning number of the local observability matrix $\mathbf{O}_\tau$ has been invoked. From the definition it naturally follows that, whenever $rang(\mathbf{O}_\tau) < n$, there exist a linear subspace of the ASV state space with zero practical excitabilty metric.

5. SUBORBITAL ROCKET EXPERIMENTAL DATA ANALYSIS.

The above concepts were applied to a CONAE navigation and control experimental payload on board a Brazilian VS30 sounding rocket having a tactical IMU (Systron Donner Motion-Pack 3 accelerometers and three gyros) sampled at 100 Hz and a GPS receiver delivering ECEF position at 1 Hz.

5.1. *The trajectory description.*

An analytic trajectory defined for any time t was synthesised (by means of the approach proposed by Giribet et al. (2007) mentioned above) to fit the actual flight data. Figure 1 shows the X components, aligned with the rocket axis, of the synthetic specific force and angular rate, and evidences the different flight stages.

The vehicle stood on the launching pad until t = 18 s. During propulsion (18 s < t < 46 s) it attained a maximum acceleration of 110 m/s^2 while being spun aerodynamically. At t = 46 s, the thrust was turned off, changing the sign of the axial acceleration due to residual air friction. An almost free flight stage (nearly null specific force) started at t = 60 s above 40 km above sea level. At t = 73 s a de-spin mechanism was activated reducing the axial angular rate by a half. The atmospheric reinsertion phase, not shown in the figure, started a few seconds later.

5.2. *The ASV deviation equations.*

The ASV $\boldsymbol{\chi} \in \mathbb{R}^{21}$ in Equation (3) includes the kinematic state $\mathbf{x} \in \mathbb{R}^9$ (referred to ECEF) and the IMU's parameters vector $\mathbf{p}_i \in \mathbb{R}^{12}$ (six biases plus six scale factors). Also $\xi \in \mathbb{R}^{21}$ while $\boldsymbol{\eta}_k \in \mathbb{R}^3$ is the GPS position error measurement. The ASV deviation vector in Equation (4) is defined as (sub-indices *a* and *b* stand, respectively, for accelerometer and gyro):

$$\begin{aligned} \delta\boldsymbol{\chi} &\triangleq \left[\delta\mathbf{P}^{eT}\ \delta\mathbf{V}^{eT}\ \delta\boldsymbol{\theta}_{be}^T\ \delta\mathbf{p}_i^T\right]^T \in \mathbb{R}^{21}; \\ \delta\mathbf{p}_i &= \left[\delta\mathbf{b}_g^T\ \delta\mathbf{b}_a^T\ \delta\mathbf{s}_g^T\ \delta\mathbf{s}_a^T\right]^T \in \mathbb{R}^{12} \end{aligned} \tag{23}$$

The specific time varying matrices in Equations (4) and (5), given below, are used as stated in Section 2 to obtain the stochastic discrete time Equation (8) used in the EKF fusion filter.

$$\mathbf{A}(t) = \left[\begin{array}{c|c|c} \mathbf{A}_{kim} & \mathbf{B}_{kin} & \mathbf{B}_{\mathbf{p}_i} \\ \hline \multicolumn{3}{c}{\mathbf{0}_{12\times 21}} \end{array}\right]; \mathbf{B}(t) = \mathbf{B}_{\mathbf{p}_i}; \mathbf{H}_k = \left[\begin{array}{c|c} \mathbf{I}_{3\times 3} & \mathbf{0}_{3x18} \end{array}\right] \tag{24}$$

https://doi.org/10.1017/S0373463319000328 Published online by Cambridge University Press

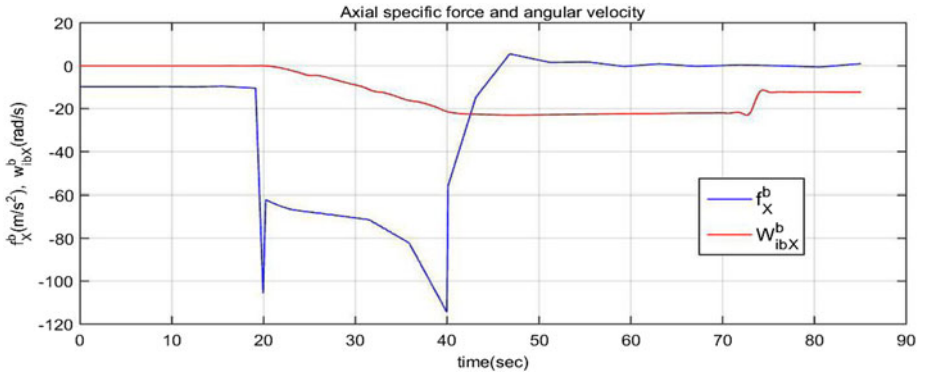

Figure 1. Axial specific force and angular velocity.

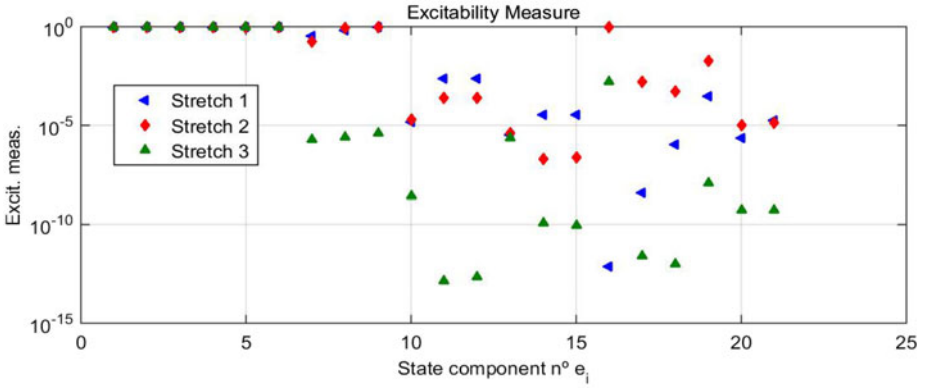

Figure 2. Excitability metric on intervals τ_1, τ_2 and τ_3.

5.3. *Analysis of the excitability metric.* We distinguish between three main trajectory segments. τ_1 = [0s, 19s]: Prior to blast-off with ECEF acceleration constant equal to local gravity at the launch pad; τ_2 = [19s, 60s]: powered flight induces changes in linear acceleration and angular rate due to aero dynamical spinning; τ_1 = [60s, 86s]: propulsion is cut off leading to a free fall motion flight. Figure 3 shows the excitability measurements obtained through each of these segments for each of the 21 components of the ASV for the threshold assumed value in Equation (20).

The above results allow us to draw the following conclusions:

- The position and velocity vectors ($\mathbf{e}_1$ to $\mathbf{e}_6$) are mostly contained in the S_O subspace and are thus observable on the three stretches. This is a natural consequence of the GPS measurements.
- The attitude vector ($\mathbf{e}_7$ to $\mathbf{e}_9$) is fundamentally contained in S_O during τ_1 and τ_2 but it almost does not excite the innovations during τ_3. As seen in España (2017) (Section 6.6.3), gravity and Earth rotation rate enable the vehicle's attitude to excite the innovations even when at rest over the Earth's surface. For the given instrumentation configuration (GPS + IMU) gravity and propulsion becomes thus necessary (but not sufficient as we will see next) for attitude estimation.

https://doi.org/10.1017/S0373463319000328 Published online by Cambridge University Press

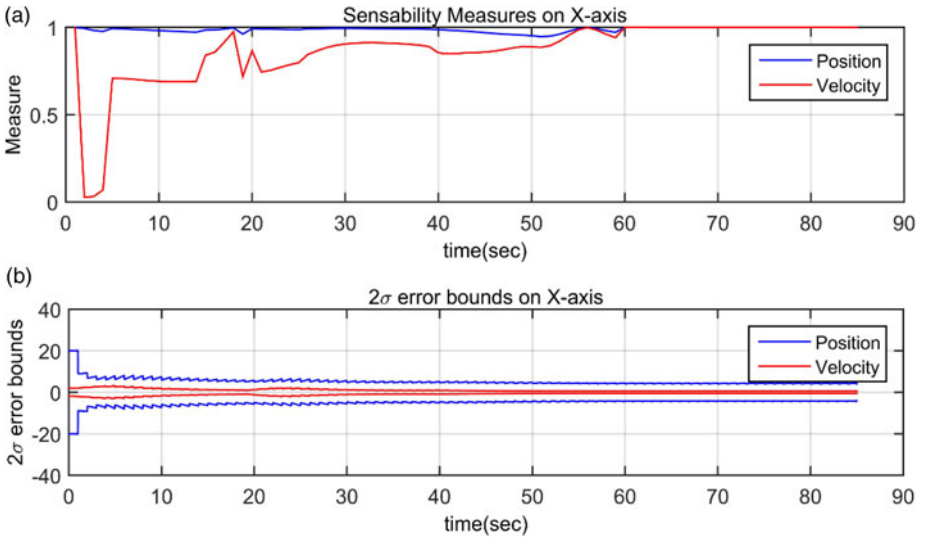

Figure 3. (a) Sensability metrics of position and velocity on the ECEF x-axis; (b) 2-σ bounds estimation errors over the x-axis.

- The scale factor of the x-gyro in body coordinates $\mathbf{e}_{16}$ becomes "excitable" during τ_2 due to the combined presence of a high acceleration and angular rate projected over that axis.
- A growth on the excitability of the x-accelerometer scale factor ($\mathbf{e}_{19}$) from τ_1 to τ_2 is once more due to the presence of propulsion. However, this fact does not seem to be enough to avoid its predominant component over S_{NO}.
- The rest of the IMU parameters have very low excitability metrics over the three segments and should thus be considered as practically unobservable for the given vehicle's trajectory. Nevertheless, one notices that biases of the excitability metric tends to be predominant over τ_1 while those of the scale factors are over τ_2.
- Finally, it can be verified that free fall is a quite unfavourable condition for in-flight IMU parameters re-calibration.

5.4. *Analysis of the sensability metric.* As seen before, the GPS position direct measure ensures almost perfectly excitable position and velocity vectors all along the trajectory. This induces a high sensability metric of the position from the very beginning and a growing tendency in the sensability of the velocity. For the assumed value $u = 0{\cdot}985$ in *Definition 1*, Figure 3(a) shows this fact for the ECEF x-components, while Figure 3(b) demonstrates how, being a measure of the available information rate, the sensabilty anticipates changes of the estimates' 2σ error band. Actually, the former is a sort of "derivative" of the latter. As such, a deep valley in the velocity sensability before t = 5 sec. induces a growth of the estimation error band, while, close to t = 12 s, the metric increase induces an error reduction. Finally, after t = 55 s the metric stabilises at its highest value ($\simeq$1) in correspondence to the lowest estimation error band of the velocity.

An exciting trajectory does not necessarily imply high sensability, but it is a required condition besides high performance instruments. Figure 2 shows that the attitude (θ_{be}) is

https://doi.org/10.1017/S0373463319000328 Published online by Cambridge University Press

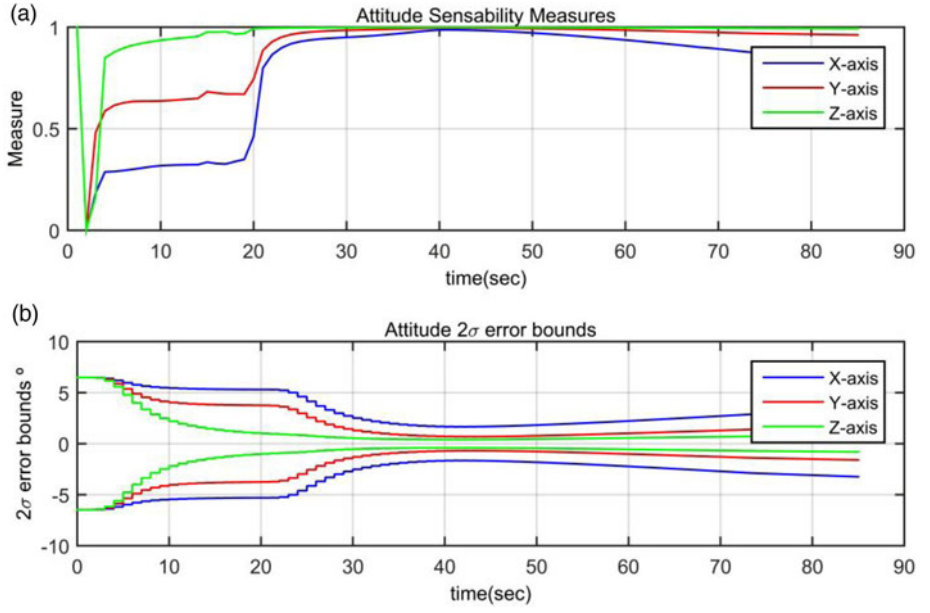

Figure 4. (a) Sensability metric of the attitude vector θ_{be}; (b) Corresponding 2-σ estimation errors bounds.

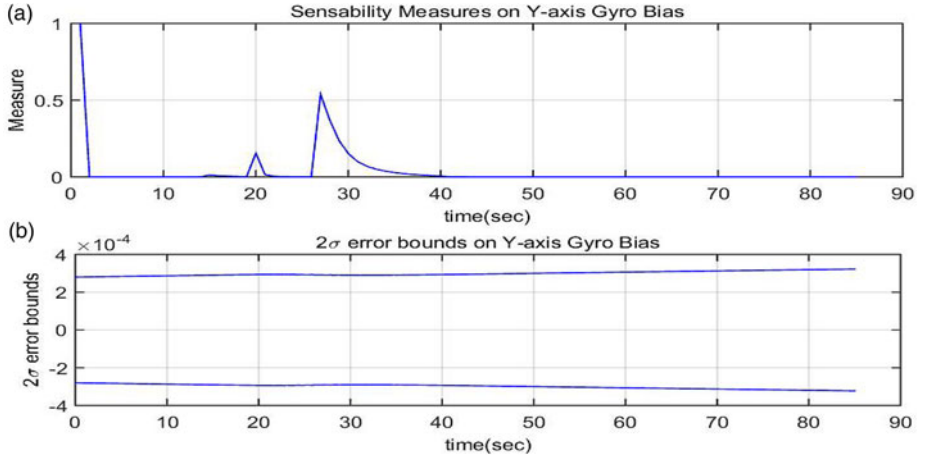

Figure 5. (a) Sensability metric of x-component of the gyro's bias and (b) its corresponding estimation error's 2-σ bounds.

highly exciting on trajectory segments τ_1, τ_2, however, as seen in Figure 4(a), the sensability of q_x and q_y only grow after blast-off (t = 19 s). While the vehicle is at rest the attitude excitability is the consequence of two vectors potentially measured by the IMU: the Earth angular rate and gravity. However, the random walk noise and bias instability levels (see España (2017)) of the tactical IMU's gyro used prevent measuring the first one and thus to take full advantage of a high excitability. Notice that, under these conditions, the IMU

https://doi.org/10.1017/S0373463319000328 Published online by Cambridge University Press

works as a mere inclinometer and thus, as shown in Figure 4(a), the θ_{be} components shall be more sensable the larger their projections are over the local tangent plane.

On the other hand, the propulsion ignition induces a boost of inertial measurements (acceleration and angular rate) within the sensitivity range of the IMU inducing a fast and sustained growth the sensability of θ_{be} during τ_2, accompanied by a reduction of its error bandwith (Figure 4(b)). At last, during free fall ($\tau_2 : t \geq 40$ s), a steady descent of the attitude sensability corresponds to a smooth increase of its error bandwidth (Figure 4(b)).

For similar reasons the IMU parameters (accelerometer and gyro biases and scale factors) turn out to be weakly sensable too. Only the y-component bias appears to be sensable but only during an interval so short in τ_2, that the filter is unable to gather enough information so as to improve its *a priori* error bound (see Figure 5(a) and 5(b)). The above result suggests that for the given trajectory and instrumentation it may be futile to try to improve the *a priori* instrument calibration during flight.

6. CONCLUSIONS. Integrated navigation systems search to estimate a vehicle's kinematics state by fusing different and independent on board measurements. As expected, the precision of the state estimates depends on measurement errors, sensors' parameters instabilities, uncertain initial conditions but, also, on the actual vehicle's trajectory.

The work proposes two novel complementary performance metrics aimed at guiding the designer in the process to evaluate the fitness of the navigation system to a family of trajectories of a given vehicle with a given on board instrument configuration. Whenever possible, the same tools would help him or her planning appropriate vehicle manoeuvres. To evaluate the aptness of a navigation system in a particular application, the designer often needs to asses which state components will be best estimated (and which will not) over a given trajectory and for a given specific sensor configuration.

Precision depends on how uncertainties "excite" the actual measurements' innovation signals. This paper formalises the concept of "excitability" together with its metric over any particular trajectory segment. In addition, an instantaneous metric quantifying the combined effects of the excitability and the involved uncertainties is also introduced called "sensabilty". As shown, an exciting trajectory does not necessarily imply high sensability of any of the state components but, it is although a required condition besides a good performing instrumentation.

The definition of practically sensable and practically observable subspaces of the state space and their corresponding orthogonal complements allows us to restrict the above measures to any specific component of the state vector. In this sense this approach may be seen as an alternative the one based on the mutual information concept proposed by Mohler and Hwang (1988).

Since real vehicles' trajectories may rarely be analytically described or even predetermined, contrary to other approaches also founded on the observability concept but using ideal analytical trajectories (circles, lemniscates, uniform acceleration, etc), we here propose an empirical method based on actual flight data.

All concepts have been illustrated with real flight data gathered on board a suborbital rocket. Its trajectory turned out to be not exciting enough to justify the recalibration of the sensors' parameters in flight. For this application, it is thus concluded that to complexify the sensor models used in data fusion algorithm will be of no assistance in terms of improving performance.

https://doi.org/10.1017/S0373463319000328 Published online by Cambridge University Press

For the sake of simplicity, the proposed excitability metric was only linked to observability and thus related with data acquired in the future of a given initial state. A similar analysis may be the pursuit using the concept of re-constructability based on past data with respect to the present state. Further research is suggested on excitability metrics based simultaneously on both concepts. Many applications using post-processed navigation (such as remote sensing systems) with non-causal filters (smoother) will greatly benefit from such an extension.

The authors are currently working in demonstrating the effectiveness of the above proposed concepts in applications with more complex trajectories and diversified instrumentation.

REFERENCES

Anderson B. D. O. and Moore, J. B. (1979). *Optimal Filtering.* Englew Cliffs, NJ: Prentice-Hall.

Bageshwar, V. L., Gebre-Egziabher, D., Garrard, W. L. and Georgiou T. T. (2009). Stochastic Observability Test for Discrete-Time Kalman Filters. *Journal of Guidance, Control and Dynamics*, **32**(4), pp. 1356–1370.

Baram, Y. and Kailath, T. (1988). Estimability and regulability of linear systems. *IEEE Transaction on Automatic Control*, **33**(12), pp. 1116–1121.

Bryson A. E. Jr. (1978). Kalman filter divergence and aircraft motion estimators. *AIAA Journal of Guidance, Control, and Dynamics*, **I**(1), pp. 71–79.

España, M. (2017). *Navegación Integrada con Aplicaciones, (Integrated Navigation with Applications)*, CONAE, 2017 https://www.argentina.gob.ar/sistemas-de-navegacion-integrada-con-aplicaciones.

Farrell, J. A. (2008). *Aided Navigation: GPS With High Rate Sensors*. , McGraw-Hill,New York, NY, USA.

Giribet, J. I., España, M. and Miranda, C. (2007). Synthetic data for validation of navigation systems. *Acta Astronautica*, **60**(2), pp. 88–95.

Giribet, J. I., Mas, I. and Moreno, P. (2018). Vision-Based Integrated Navigation System and Optimal Allocation in Formation Flying. *Proceedings of International Conference on Unmanned Aerial Systems, Dallas, USA*. pp. 52–61.

Ham, F. M. and Brown, R. G. (1983). Observability, Eigenvalues and Kalman Filtering. *IEEE Transaction on Aerospace and Electronic Systems*, **19**(2), pp. 269–273.

Hoo, S., Lee, M. H., Chun, H., Kwon, S. and Speyer, J. L. (2005). Observability of Error States in GPS/INS Integration. *IEEE Transactions on Vehicular Technology*, **54**(2), pp. 731–743.

Jazwinski, A. H. (1970). *Stochastic processes and filtering theory*, Acadademic Press, New York.

Krener A. J. and I. Kayo, Measures *of Unobservability*, 48th IEEE CDC, Shanghai, China, Dec. 16–18, 2009.

Mohler, R.R. and Hwang, C.S. (1988). Nonlinear Data Observability and Information. *Journal. of the Franklin Institute*, **325**(4), 443–464.

Moore, B.C. (1981). Principal Components Analysis in Linear Systems: Controllability, Observability and Model Reduction. *IEEE Transactions on Automatic Control*, **26**(1), pp. 17–32.

Rhee, I., Abdel-Hafez, M. F. and Speyer, J. L. (2004). Observability of an Integrated GPS/INS During Maneuvers. *IEEE Transactions on Aerospace and Electronic Systems*, **40**(2), pp. 526–535.

Shen, K., Xia, Y., Wang, M., Neusypin, K. A. and Proletarsky, A. V. (2018). Quantifying Observability and Analysis in Integrated Navigation. *Journal of the Institute of Navigation*, **65**(2), pp. 169–181.

Salychev, O.S. (1998). *Inertial systems in navigation and geophysics.* Moscow: Bauman MSTU Press.

Starks, H. and Woods, J. W. (1994). *Probability, Random Processes and Estimation Theory for Engineers.* Prentice Hall, New Jersey.

Tang, Y., Wu, Y., Wu, M., Wu, W., Hu, X., Shen, L. (2009). INS/GPS Integration: Global Observability Analysis. *IEEE Transaction on Vehicular Technology*, **58**(3), pp. 1129–1142.

Willems, J. and Mitter, S. K. (1971). Controllability, Observability, Pole Allocation and State Reconstruction. *IEEE Transaction on Automatic Control*, **16**(6), pp. 582–595.